


Nonlinear Electromagnetic Stabilization of Plasma Microturbulence

G. G. Whelan,^{1,*} M. J. Pueschel,^{2,1} and P. W. Terry¹

¹*Department of Physics, University of Wisconsin–Madison, Madison, Wisconsin 53706, USA*

²*Institute for Fusion Studies, University of Texas at Austin, Austin, Texas 78712, USA*

 (Received 20 October 2017; revised manuscript received 26 February 2018; published 27 April 2018)

The physical causes for the strong stabilizing effect of finite plasma β on ion-temperature-gradient-driven turbulence, which far exceeds quasilinear estimates, are identified from nonlinear gyrokinetic simulations. The primary contribution stems from a resonance of frequencies in the dominant nonlinear interaction between the unstable mode, the stable mode, and zonal flows, which maximizes the triplet correlation time and therefore the energy transfer efficiency. A modification to mixing-length transport estimates is constructed, which reproduces nonlinear heat fluxes throughout the examined β range.

DOI: 10.1103/PhysRevLett.120.175002

Thermal losses caused by turbulence are a major impediment to achieving controlled fusion in magnetic confinement devices. While losses can be limited through the design of large-scale devices, the cost increases commensurately, and transport control in the form of an edge transport barrier is still required. Barrier and transport control strategies require a thorough understanding of the turbulent state that develops from plasma instabilities. A key milestone in understanding turbulence (and a means for finding successful control strategies) has been the development of models capable of predicting turbulent plasma behavior and its transport. Part of this effort is to incorporate the physics insights gained into more practical reduced models.

One operating regime, desirable for fusion because it raises the fusion energy gain and enhances self-generated confining currents, is high β , where $\beta = 8\pi n_{e0}T_{e0}/B_0^2$ and n_{e0} , T_{e0} , and B_0 are equilibrium values of electron density, temperature, and magnetic field, respectively. This regime involves electromagnetic fluctuations and is of additional interest, because it exposes shortcomings both in the understanding of turbulent transport and in reduced models used for producing quick predictions of turbulent flux levels. The most familiar examples of the latter are quasilinear mixing-length transport models.

The impact of β on confinement is not entirely clear, with different experiments showing different scalings [1–3]. Moreover, the effect of β on different microturbulence regimes varies, decreasing transport in ion-temperature-gradient-driven (ITG) turbulence while increasing transport in trapped-electron-mode turbulence [4–7]. Fast ions can further reduce ITG turbulence [8,9]. Note that here *electromagnetic effects* refers to the sum of all nonequilibrium finite- β physics, including the direct impact in Ampère’s law from the plasma current and the effect on fluctuations by particle streaming along perturbed fields.

A difficult aspect of the reduction of ITG turbulence with β is that it cannot be explained by the effects of the

instability alone. This is a problem for quasilinear transport models, which are based on the instability’s properties. Quasilinear transport models are semiheuristic, with fluxes constructed dimensionally from the instability growth rate and a fluctuation scale, but with an overall level set from a nonlinear simulation [10,11]. Different quasilinear models are distinguished by their refinements to this approach [12,13]. The attractiveness of quasilinear models lies in their low computational cost compared to nonlinear simulations. However, they make implicit assumptions about the saturation physics, and one cannot generally predict their validity. The quasilinear electrostatic ion heat flux Q_i^{es} in normalized units for tokamak geometry [11,14,15]:

$$Q_i^{\text{es}} = \omega_{Ti} \mathcal{C} \sum_k \frac{w_k \gamma_k}{\langle k_{\perp}^2 \rangle}, \quad (1)$$

$$\langle k_{\perp}^2 \rangle = k_y^2 \left(1 + \hat{s}^2 \frac{\int \vartheta^2 |\Phi_k(\vartheta)|^2 d\vartheta}{\int |\Phi_k(\vartheta)|^2 d\vartheta} \right), \quad (2)$$

is described by Fick’s law as a diffusion coefficient multiplied by the normalized ion temperature gradient $\omega_{Ti} = -(R_0/T_{i0})(dT_{i0}/dx)$, R_0 is the major radius, x is the radial coordinate, and T_{i0} is the ion temperature. The diffusion coefficient depends on a scalar model constant \mathcal{C} , the linear growth rate spectrum γ_k , and an effective perpendicular wave number $\langle k_{\perp}^2 \rangle$. The latter depends on the binormal wave number k_y , normalized magnetic shear $\hat{s} = (r_0/q_0)(dq/dx)$, where q_0 is the safety factor and r_0 is the radial coordinate, and the eigenmode potential $\Phi_k(\vartheta)$, where ϑ is the ballooning angle. The model is weighted by $w_k = Q_{i,k}^{\text{es}}|_{\text{lin}}/n_{i,k}^2|_{\text{lin}}$, where $Q_{i,k}^{\text{es}}|_{\text{lin}}$ is the heat flux generated by the unstable eigenmode at wave number k and $n_{i,k}^2|_{\text{lin}}$ is the square of the ion density of the same mode.

Despite their simplicity, quasilinear estimates show good agreement with nonlinear predictions for many parameter

scalings, including temperature gradients, temperature ratio, collisionality, and effective charge [15–17]. However, in the case studied here, the above quasilinear model predicts only a 50% reduction in transport between low and high β compared to a 95% reduction seen in nonlinear simulations. The quasilinear model's failure to accurately predict electromagnetic stabilization indicates that it does not include changes to the underlying saturation physics with β .

To understand the effect of β on saturated ITG turbulence, a series of diagnostic measurements in gyrokinetic simulations are performed to characterize the role of stable modes, including measurements of free energy production, nonlinear transfer, and dissipation. Stable modes are important in turbulence when their levels are sufficient to impact saturation. This generally occurs when there are stable modes with damping rates comparable to the growth rate, a condition fulfilled in numerous systems [18,19]. The extent to which stable-mode effects can be incorporated into reduced transport models is studied here for the first time. All simulations were carried out using the gyrokinetic code GENE [20,21]. We use parameters with a single unstable ITG mode for each perpendicular wave vector in the unstable range. The two-dimensional scan in β and ω_{Ti} follows parameters in Ref. [6]. If not labeled otherwise, all plots are for $\omega_{Ti} = 8$, though conclusions hold for all temperature gradients investigated here ($\omega_{Ti} = 6, 7, 8$).

The free energy for species j is given by [22]

$$E_k = \text{Re} \left[\int dz d\mathbf{v} \frac{n_{j0} T_{j0}}{F_{j0}} \left(g_{jk} + \frac{q_j F_{j0}}{T_{j0}} \chi_{jk} \right)^* g_{jk} \right], \quad (3)$$

where $-\pi \leq z < \pi$ is the parallel coordinate, F_{j0} is the background Maxwellian distribution, q_j is the species charge, and $g_{jk} = f_{jk} + (2q_j/m_j v_{Tj}) v_{\parallel} \bar{A}_{\parallel} F_{j0}$ is the modified distribution function, depending on the distribution function f_{jk} , the species mass m_j , the thermal velocity of the species of interest v_{Tj} , the velocity parallel to the magnetic field v_{\parallel} , and the parallel component of the gyroaveraged magnetic vector potential \bar{A}_{\parallel} . The modified potential $\chi_j = \bar{\Phi} - v_{Tj} v_{\parallel} \bar{A}_{\parallel}$ depends on the gyroaveraged potential $\bar{\Phi}$. For $\beta \ll 1$, parallel magnetic fluctuations δB_{\parallel} are small and neglected here.

Gyrokinetic models have many eigenmodes at every wave number whose nonlinear excitation can introduce scalings outside the normal dependencies of the quasilinear theory. These eigenmodes, which span the phase space of velocity and parallel displacement, are roots of the linear gyrokinetic operator. Spectral energy transfer couples eigenmodes through the $\mathbf{E} \times \mathbf{B}$ nonlinearity, which transfers energy within wave number triplets according to the condition $\mathbf{k} - \mathbf{k}' = \mathbf{k}''$. The energy transfer rate to Fourier wave number $\mathbf{k} = (k_x, k_y)$ due to coupling with \mathbf{k}' and \mathbf{k}'' is

$$T_{k,k'} = 2\text{Re} \left\{ \int dz d\mathbf{v} \frac{n_{j0} T_{j0}}{F_{j0}} \left[g_{jk} + \frac{q_j F_{j0}}{T_{j0}} \chi_{jk} \right]^* \times [(\mathbf{k} \times \mathbf{k}') \cdot \hat{\mathbf{b}}] \left[\chi_j(k') g_j(k'') \right] \right\}. \quad (4)$$

This function is decomposed so that it tracks transfer to individual eigenmodes, revealing that electrostatic ITG turbulence saturates through zonal-flow-mediated energy transfer to higher radial wave numbers and stable modes at the same scales as the instability [23–25]. Zonal flows [5] and stable modes [26] are known to be susceptible to finite- β effects; hence, the decomposition of $T_{k,k'}$ is analyzed to determine their role in saturation.

The inclusion of electromagnetic effects does not qualitatively change the saturation mechanisms. From the decomposition of Eq. (4) for the wave numbers that have the highest energy injection rate, which are responsible for the most flux, roughly 90% of the energy transfer is mediated by fluctuations at the zonal wave number $k_y = 0$. Several percent of this energy is deposited into the zonal mode, and the rest goes to the higher- k_x mode. Energy transfer to the unstable and stable eigenmodes at the higher- k_x mode in the triplet is comparable.

The large number of stable modes makes tracking their individual amplitudes numerically infeasible, and the effects of stable modes on the turbulence are complicated by their widely differing damping rates and mode structures, as well as mode nonorthogonality. A simpler analysis technique is to decompose the distribution function at a wave number into the unstable mode and a remainder spanned by stable modes.

Figure 1 shows the energy transfer rate to the higher- k_x mode due to coupling to a zonal mode responsible for a significant energy transfer with $k_x = 0.083$, split into a transfer to the unstable eigenmode T_{ZF}^U and the remainder T_{ZF}^S of the combined stable modes. In Eq. (4), this is equivalent to choosing $\mathbf{k}' = (0.083, 0)$ and decomposing g_k into the unstable mode and a remainder spanned by stable modes. The energy transfer rate to stable modes is negative for the lowest k_x wave number, because

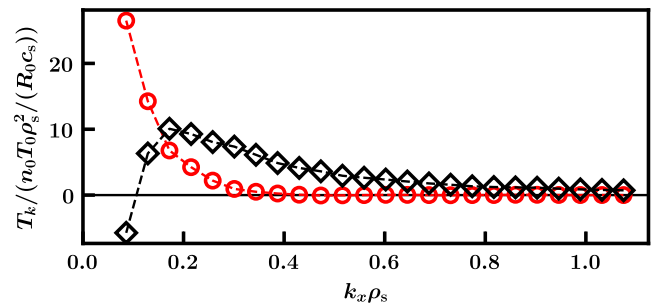


FIG. 1. Zonal-flow-catalyzed energy transfer to unstable modes T_{ZF}^U (red circles) and stable modes T_{ZF}^S (black diamonds) at $k_y \rho_s = 0.4$ as a function of the radial wave number.

nonorthogonality enhances energy production; this is described later in the section on effective growth rates. The decline in the energy transfer rate is related to stable mode dissipation, which can be measured by summing over all the couplings, and is approximated here with a sum over zonal couplings. At $k_y = 0.4$, stable modes dissipate 70% of the energy produced by the unstable modes up to the end of the unstable range at $k_x = 0.25$, while at $k_y = 0.2$, their net effect enhances the energy production by 20% in the same range.

Individual terms of the nonlinearity make different contributions to the saturation of the instability. The free energy [see Eq. (3)] is the sum of terms proportional to $\|g\|^2/F_0$ and χ^*g , an entropylike and a wave-energy term, respectively. The transfer of entropy ($\propto g_k\chi_{k'}g_{k''}$) was found to be larger by more than an order of magnitude than that of field energy ($\propto \chi_k\chi_{k'}g_{k''}$) at all β . This mirrors the electrostatic case, where entropy is similarly larger than wave energy [27]. However, the wave-energy contribution grows with β .

The catalytic zonal mode $\chi_{k'}$ of the nonlinearity ($k'_y = 0$) can be split into electrostatic and electromagnetic components proportional to $\bar{\Phi}$ and \bar{A}_{\parallel} . Energy transfer can be decomposed similarly. Energy transfer from the electromagnetic term ($\propto g_k\bar{A}_{\parallel,k'}g_{k''}$) was found to scale with β and to generally be negative several percent of that from its electrostatic counterpart ($\propto g_k\bar{\Phi}_{k'}g_{k''}$).

The projection of the turbulent distribution function g_{nl} onto the linearly unstable ITG eigenmode g_{lin} determines the extent to which the turbulence is represented by the unstable mode. The projection is given by

$$P(g_{nl}, g_{lin}) = \frac{\|g_{nl}(z, \mathbf{v}) \cdot g_{lin}(z, \mathbf{v})\|}{\|g_{nl}\| \|g_{lin}\|}. \quad (5)$$

The projection can take values between 0 and 1, with 0 meaning the distribution function is perfectly described by a sum of stable eigenmodes, while for 1 it is perfectly described by the unstable eigenmode.

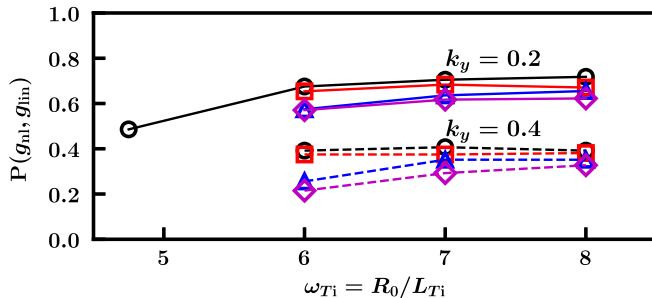


FIG. 2. Temperature gradient dependence of the unstable mode fraction $P(g_{nl}, g_{lin})$ at two wave numbers in the saturated turbulent state. Plotted are $\beta = 0.01\%$ (black circles), $\beta = 0.25\%$ (red squares), $\beta = 0.5\%$ (blue triangles), and $\beta = 0.75\%$ (magenta diamonds). The two wave numbers are $k_y\rho_s = 0.2$ (solid line) and $k_y\rho_s = 0.4$ (dashed lines).

Figure 2 shows the time average of $P(g_{nl}, g_{lin})$ at two wave numbers as a function of ω_{Ti} and β . The mode at $k_y = 0.2$ is around the peak in transport, while $k_y = 0.4$ is closer to the peak in the growth rate. Stable mode excitation is enhanced with β and depends strongly on perpendicular wave number, consistent with the results depicted in Fig. 1. The turbulent distribution function at low k_y resembles the unstable mode, decreasing its corresponding contribution from 75% to 60% as β increases from 0.01% to 0.75%. At higher k_y , the unstable mode contribution changes from around 40% to 35% over the same range in β .

Measuring the stable mode fraction alone misses the effect of stable modes on energy production and dissipation, which cannot be inferred from the amplitude alone, as many modes simultaneously make differing contributions. The normalized energy production rate provides a quantitative measure of the net effects of stable modes on the energy.

For energy production, consider an effective nonlinear growth rate defined as

$$2\gamma_{\text{eff}} = \frac{dE_k/dt|_{\text{NC}}}{E_k}, \quad (6)$$

where $dE/dt|_{\text{NC}}$ represents the energy change arising from nonconservative terms [28–30], which can be compared directly to the growth rate of the unstable mode γ_{ITG} for a measure of the role of stable modes in saturation. If stable modes are not excited in saturation, the effective growth rate γ_{eff} is equal to γ_{ITG} .

Figure 3 compares γ_{eff} with γ_{ITG} at two β values. Near $k_y = 0.1$, i.e., around the peak in transport and energy production, γ_{eff} follows and even slightly exceeds γ_{ITG} . Where γ_{eff} exceeds γ_{ITG} , the stable mode contribution boosts energy production by increasing $g_k^*i k_y \chi_k$. Higher wave numbers show decreased γ_{eff} , with net energy dissipation in the tail of the linearly unstable range. The relative change mimics the unstable mode proportion; where the distribution function is well described by the unstable mode, γ_{eff} follows γ_{ITG} closely, while increased stable mode excitation at a higher wave number brings γ_{eff} down significantly. While stable modes and their effect on

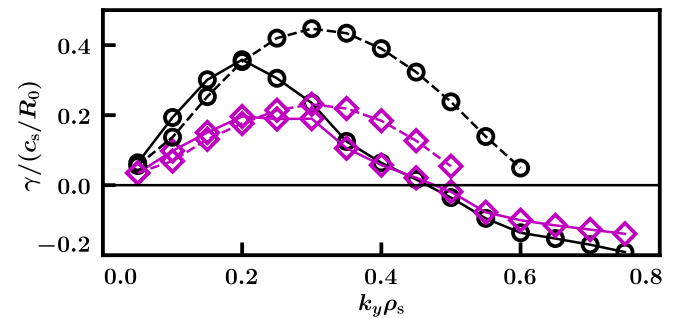


FIG. 3. Spectrum of the nonlinear γ_{eff} (solid lines) and the linear γ_{ITG} (dashed lines) at $\beta = 0.01\%$ (black circles) and $\beta = 0.75\%$ (magenta diamonds).

the energy are always seen to be important in saturation, their impact does not change much with β . The increase in stable mode excitation is only equivalent to a decrease in the growth rate of 10%–20%, compared to the 90% reduction relative to quasilinear flux, so increased stable mode excitation is only a secondary player in the heat flux β scaling.

The direction and magnitude of the energy transfer depends on the relative phase between modes within a triplet; the time-averaged transfer depends on their correlation. Eddy-damped quasilinear Markovian closures [31] predict that energy transfer rates are proportional to $\hat{G}\tau$, where \hat{G} depends on coupling coefficients and products of energy quantities, and the triplet correlation time $\tau = -i[\hat{\omega}'' + \hat{\omega}' - \hat{\omega}^*]^{-1}$ relates to the time modes spend in phase [30,32,33]. A recent analytical calculation of the saturation of toroidal ITG in a fluid model [34] shows that saturated turbulent amplitudes scale inversely with τ , and maximizing τ is currently being investigated for stellarator turbulence optimization studies [35]. Because the energy transfer rate scales with τ , it can be thought of as a nonlinear efficiency, where the highest τ , corresponding to the resonance of the three frequencies, allows smaller mode amplitudes to match the energy injected by the instability. Formally, τ is the timescale associated with the nonlinear response to an impulse; when τ is small, the system has a limited memory of interaction. The nonlinear frequency $\hat{\omega}$ for a mode at \mathbf{k} can be expressed as the linear frequency with nonlinear corrections due to the interactions with other modes. It can be measured directly from the Fourier transform of the temporal autocorrelation function of $\tilde{\Phi}_{\mathbf{k}}$ [36]. A common fitting assumption is that this follows a Lorentzian or Gaussian with peak at the real frequency and width corresponding to the eddy damping rate [37].

Figure 4 shows $|\tau|$ for zonal couplings to the mode which causes the most energy production and transport. The quantity $|\tau|$ is highest for coupling to modes at a low

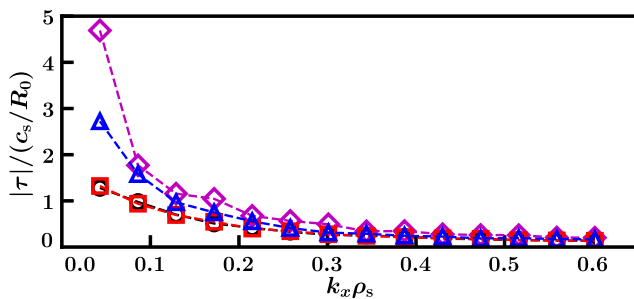


FIG. 4. The absolute value of the triplet correlation time $|\tau|$ is calculated for triplets involving the mode at $k_y \rho_s = 0.15$ and zonal flows at individual $k_x \rho_s$, for $\beta = 0.01\%$ (black circles), $\beta = 0.25\%$ (red squares), $\beta = 0.50\%$ (blue triangles), and $\beta = 0.75\%$ (magenta diamonds). A clear increase of nonlinear efficiency with β is observed, which is responsible for most of the nonlinear stabilization due to finite β .

radial wave number, which energy transfer analysis reveals to be those with the dominant energy transfer rates. Increasing β from 0.01% to 0.75% doubles $|\tau|$, underscoring that the nonlinear correlation effect is significantly more impactful on nonlinear electromagnetic stabilization than the stable mode effect as measured by the unstable mode partition or the energy production rate.

Measurements of τ from nonlinear simulations are too computationally involved for quick predictions. As a linear proxy, we consider $\tau_{\text{lin}} = -i[\omega_{\text{ITG}}'' - \omega_{\text{ITG}}^*]^{-1}$, which measures the triplet correlation lifetime between two unstable eigenmodes and an undamped, zero-frequency zonal flow. The β scaling of this proxy is similar to that of the fully nonlinear quantity in the wave number region of interest, seen implicitly from Fig. 5. Larger β extends the mode structure [38] and increases $|\tau|$ by reducing the dependence of γ on k_x . The quantity τ_{lin} differs from τ , because it represents the first step in a cascade to a higher wave number instead of direct coupling to a dissipation mechanism, and it lacks nonlinear frequency corrections. The effect of nonlinear frequency corrections and stable modes on τ will be discussed in a subsequent paper.

Now we discuss the heat flux scaling, its modeling by the quasilinear formula Eq. (1), and the effect of the nonlinear properties mentioned above. Figure 5 compares the quasilinear scalings of $\sum \gamma_k / k_{\perp}^2$, $\sum w_{j,k} \gamma_k / \langle k_{\perp}^2 \rangle$, $\sum |\tau_{\text{nl},k}|^{-1} w_{j,k} \gamma_k / \langle k_{\perp}^2 \rangle$, $\sum |\tau_{\text{lin},k}|^{-1} w_{j,k} \gamma_k / \langle k_{\perp}^2 \rangle$, and nonlinear flux Q_i^{es} with β at $\omega_{Ti} = 8$. The nonlinear heat transport is reduced by roughly a factor of 20 over this range in β . In comparison, the growth rate decreases by less than half. Incorporating the proper weights with a perpendicular scale ($\langle k_{\perp}^2 \rangle$ vs k_{\perp}^2) and normalized transport w_k lowers transport predictions 30% as structures broaden with β . The model that scales inversely with $|\tau_{\text{nl},k}|$ predicts an 80% stabilization, which is much closer to the nonlinear results. With $\omega_{Ti} = 6$ ($\omega_{Ti} = 7$), the quasilinear model

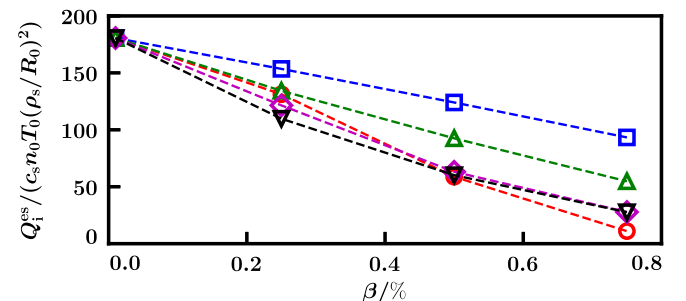


FIG. 5. Normalized heat flux (red circles) as a function of β , compared to the following quasilinear models: $\sum \gamma_k / k_{\perp}^2$ (blue squares), $\sum w_{j,k} \gamma_k / \langle k_{\perp}^2 \rangle$ (green upwards triangles), $\sum |\tau_{\text{nl},k}|^{-1} w_{j,k} \gamma_k / \langle k_{\perp}^2 \rangle$ (magenta diamonds), and $\sum |\tau_{\text{lin},k}|^{-1} w_{j,k} \gamma_k / \langle k_{\perp}^2 \rangle$ (black downwards triangles). All quasilinear data use model constants such that the nonlinear flux is matched in the electrostatic limit.

predicted a 70% (60%) reduction in the flux, compared to the τ -modified model predicting a 95% (90%) with actual reductions of 99% (95%). Transport predictions are very similar between quasilinear models using linear and nonlinear τ . Whether the agreement seen in Fig. 5 is special to the case examined or more general will be investigated elsewhere. The τ proxy based on couplings between two unstable modes and a zonal flow may work well, because the balance between transfer to stable modes and unstable modes does not depend strongly on β . This model does not include the enhanced stable mode excitation with β discussed earlier, which would further reduce transport. While this modification constitutes a clear improvement relative to existing models, one can envision cases where the inclusion of τ will not be sufficient to recover nonlinear results; such cases include changes to the stable mode dissipation [18] or multiple unstable eigenmodes. Experimental parameter sets with collisional dissipation will be addressed in further work. These findings demonstrate the importance of τ as a fundamental contributor in nonlinear energy transfer.

To summarize the findings of this Letter, we note that, qualitatively, electromagnetic effects do not change ITG saturation physics. Energy production due to the instability is balanced by a transfer to higher-radial-wave-number unstable and stable modes. The latter changes energy production, increasing normalized energy production at low k_y and extending the unstable radial wave number range, while at higher binormal wave numbers providing a stabilizing effect.

Electromagnetic effects strongly reduce transport from ITG turbulence. The majority of this effect is due to a higher triplet correlation time $|\tau|$, which can be thought of as an efficiency factor in the nonlinearity. Quasilinear transport models scaled with $|\tau|^{-1}$ accurately follow nonlinear transport predictions across the investigated β range. While preliminary, linear proxies for the triplet correlation time that use eigenmode frequencies show promise for use in quasilinear models.

While these findings are robust throughout a wide range of temperature gradients and β , further work is in progress applying this scaling to gyrokinetic analyses of experimental β scans on multiple devices. The role of the τ in electromagnetic stabilization due to fast ions is also under investigation.

We thank J. Citrin for helpful discussions. Simulations were done at NERSC. Work supported by the U.S. Department of Energy, Office of Science, Fusion Energy Sciences, Award No. DE-FG02-89ER53291.

* ggwhelan@wisc.edu

[1] L. Vermare, F. Ryter, C. Angioni, A. G. Peeters, J. Stober, R. Bilato, L. D. Horton, B. Kurzan, C. F. Maggi, H. Meister,

- J. Schirmer, G. Tardini, and The ASDEX Upgrade Team, *Nucl. Fusion* **47**, 490 (2007).
- [2] D. C. McDonald, L. Laborde, J. C. Deboo, F. Ryter, M. Brix, C. D. Challis, P. de Vries, C. Giroud, D. Howell, E. Joffrin, T. C. Luce, J. Mailloux, V. Pericoli-Ridolfini, A. C. C. Sips, K. Thomsen, and JET EFDA Contributors, *Plasma Phys. Controlled Fusion* **50**, 124013 (2008).
- [3] C. C. Petty, *Phys. Plasmas* **15**, 080501 (2008).
- [4] J. Candy, *Phys. Plasmas* **12**, 072307 (2005).
- [5] M. J. Pueschel, M. Kramerer, and F. Jenko, *Phys. Plasmas* **15**, 102310 (2008).
- [6] M. J. Pueschel and F. Jenko, *Phys. Plasmas* **17**, 062307 (2010).
- [7] A. Ishizawa, S. Maeyama, T.-H. Watanabe, H. Sugama, and N. Nakajima, *J. Plasma Phys.* **81**, 435810203 (2015).
- [8] J. Citrin, F. Jenko, P. Mantica, D. Told, C. Bourdelle, J. Garcia, J. W. Haverkort, G. M. D. Hogeweij, T. Johnson, and M. J. Pueschel, *Phys. Rev. Lett.* **111**, 155001 (2013).
- [9] J. Citrin, J. Garcia, T. Goerler, F. Jenko, P. Mantica, D. Told, C. Bourdelle, D. R. Hatch, G. M. D. Hogeweij, T. Johnson, M. J. Pueschel, M. Schneider, and JET-EFDA Contributors, *Plasma Phys. Controlled Fusion* **57**, 014032 (2015).
- [10] M. Kotschenreuther, W. Dorland, M. A. Beer, and G. W. Hammett, *Phys. Plasmas* **2**, 2381 (1995).
- [11] F. Jenko, T. Dannert, and C. Angioni, *Plasma Phys. Controlled Fusion* **47**, B195 (2005).
- [12] G. M. Staebler, J. E. Kinsey, and R. E. Waltz, *Phys. Plasmas* **12**, 102508 (2005).
- [13] C. Bourdelle, X. Garbet, F. Imbeaux, A. Casati, N. Dubuit, R. Guirlet, and T. Parisot, *Phys. Plasmas* **14**, 112501 (2007).
- [14] M. J. Pueschel, B. J. Faber, J. Citrin, C. C. Hegna, P. W. Terry, and D. R. Hatch, *Phys. Rev. Lett.* **116**, 085001 (2016).
- [15] T. Dannert and F. Jenko, *Phys. Plasmas* **12**, 072309 (2005).
- [16] Z. Lin, I. Holod, L. Chen, P. H. Diamond, T. S. Hahm, and S. Ethier, *Phys. Rev. Lett.* **99**, 265003 (2007).
- [17] A. Casati, C. Bourdelle, X. Garbet, F. Imbeaux, J. Candy, F. Claret, G. Dif-Pradalier, G. Falchetto, T. Gerbaud, V. Grandgirard, Ö. D. Gürcan, P. Hennequin, J. Kinsey, M. Ottaviani, R. Sabot, Y. Sarazin, L. Vermare, and R. E. Waltz, *Nucl. Fusion* **49**, 085012 (2009).
- [18] D. R. Hatch, F. Jenko, A. Bññon Navarro, and V. Bratanov, *Phys. Rev. Lett.* **111**, 175001 (2013).
- [19] K. D. Makwana, P. W. Terry, J.-H. Kim, and D. R. Hatch, *Phys. Plasmas* **18**, 012302 (2011).
- [20] F. Jenko, W. Dorland, M. Kotschenreuther, and B. N. Rogers, *Phys. Plasmas* **7**, 1904 (2000).
- [21] See <http://www.genecode.org> for code details and access.
- [22] J. Candy and R. E. Waltz, *Phys. Plasmas* **13**, 032310 (2006).
- [23] C. Holland, P. H. Diamond, S. Champeaux, E. Kim, Ö. D. Gürcan, M. N. Rosenbluth, G. R. Tynan, N. Crocker, W. Nevins, and J. Candy, *Nucl. Fusion* **43**, 761 (2003).
- [24] M. Nakata, T.-H. Watanabe, and H. Sugama, *Phys. Plasmas* **19**, 022303 (2012).
- [25] K. D. Makwana, P. W. Terry, M. J. Pueschel, and D. R. Hatch, *Phys. Rev. Lett.* **112**, 095002 (2014).
- [26] D. R. Hatch, M. J. Pueschel, F. Jenko, W. N. Nevins, P. W. Terry, and H. Doerk, *Phys. Plasmas* **20**, 012307 (2013).
- [27] K. Makwana, Ph.D. Thesis, University of Wisconsin-Madison, 2013.

- [28] T.-H. Watanabe and H. Sugama, *Nucl. Fusion* **46**, 24 (2006).
- [29] D. R. Hatch, P. W. Terry, F. Jenko, F. Merz, and W. M. Nevins, *Phys. Rev. Lett.* **106**, 115003 (2011).
- [30] D. A. Baver, P. W. Terry, R. Gatto, and E. Fernandez, *Phys. Plasmas* **9**, 3318 (2002).
- [31] S. A. Orszag, *J. Fluid Mech.* **41**, 363 (1970).
- [32] K. D. Makwana, P. W. Terry, and J. H. Kim, *Phys. Plasmas* **19**, 062310 (2012).
- [33] M. Lesieur, *Turbulence in Fluids* (Kluwer Academic, Dordrecht, 1990), pp. 161–175.
- [34] P. W. Terry, B. J. Faber, C. C. Hegna, V. V. Mirnov, M. J. Pueschel, and G. G. Whelan, *Phys. Plasmas* **25**, 012308 (2018).
- [35] C. C. Hegna, P. W. Terry, and B. J. Faber, *Phys. Plasmas* **25**, 022511 (2018).
- [36] P. W. Terry and W. Horton, *Phys. Fluids* **26**, 106 (1983).
- [37] J. Citrin, C. Bourdelle, P. Cottier, D. F. Escande, O. D. Gurcan, D. R. Hatch, G. M. D. Hogeweyj, F. Jenko, and M. J. Pueschel, *Phys. Plasmas* **19**, 062305 (2012).
- [38] M. J. Pueschel, T. Goerler, F. Jenko, D. R. Hatch, and A. J. Cianciara, *Phys. Plasmas* **20**, 102308 (2013).